RLCYC 75: a 2 kW electrically calibrated laser calorimeter designed for Laser MegaJoule diagnostics calibration

C Crespy[1,4], D Villate[1,4], M Soscia[2], F Coste[3] and R Andre[1]

[1] CEA, Cesta, BP 2, 33114 Le Barp, France
[2] Laser Metrologie, ZA des Romains, 11 route de Salle, 74690 Cran-Gevrier, France
[3] PIMM, ENSAM Paris, 151, Bd de l'Hôpital, 75013 Paris, France

E-mail: charles.crespy@cea.fr and denis.villate@cea.fr

Abstract
RLCYC 75 is a new electrically calibrated laser calorimeter specially manufactured by Laser Metrology to calibrate energy diagnostics within the Laser MegaJoule (LMJ) facility. It consists of an optical cavity cooled by a hydraulic system. The system is designed to provide 1 µm wavelength power laser measurements with uncertainty less than 1% at 2 kW and traceability to the International System of Units (SI). In this paper, the accuracy of RLCYC 75 measurements is studied. More precisely, three points are detailed: instrumentation uncertainty estimation, equivalence between optical and electrical supply and light absorption. To this end, electrical calibration campaigns and power laser measurement campaigns are conducted. Moreover, thermal and optical models are developed. Results show that RLCYC 75 design and instrumentation are efficient enough to reach the goal of relative uncertainty of about 1% at 2 kW. RLCYC 75 will become the 2 kW laser power primary standard for LMJ applications.

(Some figures may appear in colour only in the online journal)

1. Introduction

The Laser MegaJoule (LMJ) facility at Commissariat à l'Energie Atomique et aux Energies Alternatives (CEA) near Bordeaux (France) is designed to achieve fusion ignition of a deuterium–tritium target. It will contain 176 square-shaped laser beams having a section of $400 \times 400\,\mathrm{mm}^2$. The wavelength during the amplification process is 1053 nm (1ω). The amplified 1ω beams are frequency converted to 351 nm (3ω) before reaching the target. The energy transported by a beam is close to 10 kJ and the pulse duration is close to 3 ns. A detailed description of the LMJ facility can be found in [1–3]. The laser pulse energy measurement is a key point in LMJ applications. In fact, the absolute uncertainty on the total energy measurement has to be less than 2%. To calibrate the laser energy diagnostics of LMJ, a 2 kW continuous wave (cw) laser power standard at 1 µm wavelength is required to relate the energy measurement to the International System of Units (SI) with an uncertainty of less than 1%.

[4] Authors to whom any correspondence should be addressed.

Many national metrology institutes have developed traceability chains to perform absolute laser power measurements. The first element of the chain is a calorimeter used as the primary standard. Since optical power is usually linked to the SI units through an electrical standard, these calorimeters are calibrated against a primary electrical standard. Brandt *et al* report the whole traceability chain used for laser power standard at Physikalisch Technische Bundesantalt (PTB, Germany) in [4]. The primary standard used at PTB is a cryogenic calorimeter designed for 1 mW laser power measurement. The uncertainty due to the primary standard calorimeter is very low (0.01%); nonetheless, the traceability chain leads to an important enhancement on uncertainty for 120 W power measurements (0.4%).

Li *et al* report a comparison of high laser power measurements between PTB and the National Institute of Standards and Technology (NIST, USA) (see [5]). The relative discrepancy in the measurements is 0.5%. In order to perform accurate high laser power (120 W at 1 µm) measurements, the NIST uses laser traceability chains involving different types of calorimeters and calibrated beam splitters. The primary

standard used at the NIST is a K-series calorimeter providing 60 W measurement at 1 µm. In [6], the authors deal with non-linearity sources of high-power laser detectors, which enhance the uncertainty of the traceability chain. The authors review the non-linearity sources inherent to thermal detectors: radiation losses and non-linear behaviour of temperature sensors. The uncertainty of the NIST high-power laser detector calibration including non-linearity is found to be 1.3%. A review of the high-power laser measurement standards at the NIST is presented in [7].

Since a traceability chain from 50 W to 2 kW would lead to an important uncertainty, it is chosen to develop a 2 kW electrically calibrated primary standard calorimeter for calibration of LMJ diagnostics. In this configuration, the traceability chain is reduced to the simplest form: it just involves the calibration of laser power measurement against an electrical standard. Our 2 kW electrically calibrated laser calorimeter is called RLCYC 75. It is designed and manufactured by *Laser Métrologie*®. The RLCYC 75 principle is inspired by the calorimeters developed at the Laboratoire National d'Essais (LNE, France) for the EuroLaser EU194 program in 1988 (see [8]). It consists of an optical cavity cooled by a hydraulic system. In this paper, the purpose is to quantify the absolute uncertainty of RLCYC 75 measurements.

Concerning electrically calibrated calorimeter measurements, two kinds of uncertainty contributors must be distinguished (see [9, 10]).

- Some uncertainty sources are linked to the instrumentation: uncertainty on electrical power dissipated, temperature probes, etc.
- Some others are connected to the calorimeter design: light absorption or thermal non-equivalence (difference in temperature response between optically delivered power and electrically delivered power).

Thus, to improve measurement accuracy, calorimeters have to be designed in order to reduce the thermal non-equivalence and to enhance the light absorption. This point has been the aim of many works over the last 30 years (see [11–14]). To illustrate this point, it is noteworthy that the main interest of using a cryogenic calorimeter as the primary standard is the thermal equivalence at a low laser power (about 1 mW) (see [15–17]). Generally, thermal non-equivalence is estimated by modelling the thermal behaviour of the calorimeter (see [18, 19]).

Therefore, to quantify the uncertainty of RLCYC 75, not only should the performances of the instrumentation be validated, but also the calorimeter design.

To this end, experimental campaigns have been conducted to study the statistical uncertainties linked to the instrumentation. Moreover, numerical tools have been developed.

- Light absorption is modelled using a Monte Carlo type ray-tracing model.
- A 3D thermal model is implemented to quantify the thermal equivalence between optical and electrical supply.

This paper is organized as follows. In the second section, the RLCYC 75 measurement principle is presented. The uncertainty due to the measurement procedure is examined in section 3 (uncertainty due to the primary electrical standard and due to instrumentation). In section 4, the uncertainty linked to electrical losses is studied. Section 5 deals with the uncertainty due to incomplete electrical and light absorption. Section 6 is about thermal non-equivalence estimation. In section 7, the global uncertainty on absolute laser power measurements is discussed.

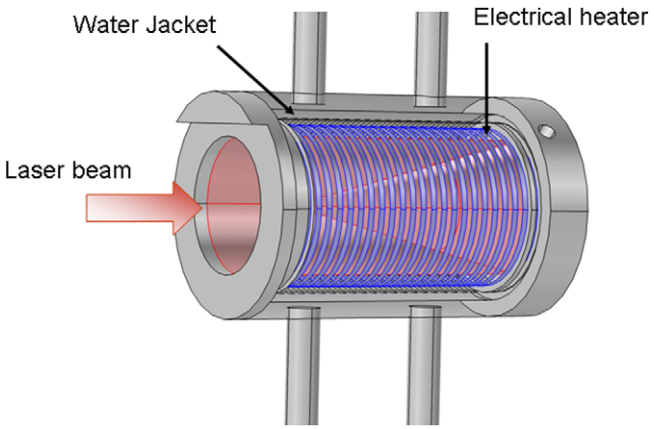

Figure 1. Schematic of the RLCYC 75 calorimeter.

2. RLCYC 75 calorimeter

2.1. Presentation

A schematic of the RLCYC 75 calorimeter is presented in figure 1. It consists of a copper cylindro-inner-cone cavity cooled by an internal heat exchanger (water jacket). The aperture of the cavity is 75 mm. The surface of the cavity is painted with a carbon-absorbing coating. The cavity is designed for divergent square-shaped laser beam absorption (which is an important point for calibration of LMJ diagnostics). In order to increase its performance, the hydraulic cooling system consists of an optimized square-shaped exchanger (section $6 \times 8\,\mathrm{mm}^2$). The total length of the heat exchanger is 4.8 m.

To perform a laser power measurement, two measurements are required: the flow rate (q) and the water temperature increase along its path in the calorimeter (ΔT). The power absorbed by the calorimeter (P) is thus estimated using the equation

$$P = C_e \cdot q \cdot \Delta T, \tag{1}$$

where C_e is the calibration coefficient; it is close to the water thermal capacity at constant volume. To perform laser power measurements traceably to SI units, electrical calibrations must be achieved. To this end, an electrical heater is installed within the calorimeter. It is a 6 m long bifilar element sheathed with ICONEL 600 (resistance 40 Ω). Electrical link is made through cold extremities. It is manufactured by THERMOCOAX®. The electrical heater is housed in the grooves situated on the outer surface of the cylinder. Thus, C_e

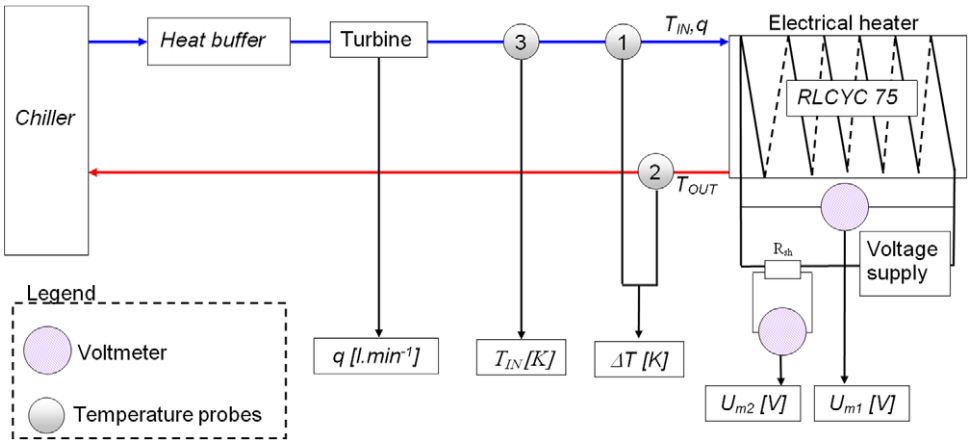

Figure 2. Schematic of the instrumentation and the hydraulic system used for RLCYC 75 measurements.

is estimated during electrical calibration with the equation

$$C_e = \frac{P_e}{q \cdot \Delta T}, \tag{2}$$

with P_e the electrical primary standard.

The instrumentation and the hydraulic system for RLCYC 75 measurements are shown in figure 2 and detailed in the following.

2.2. Hydraulic system

The hydraulic system consists of a chiller paired with a thermal buffer. The temperature of the water from the chiller is regulated at ±0.1 °C, using injection of hot gases. The thermal tank volume is 120 l. To reach the required performance, a heat buffer is employed within the hydraulic system. It is a heat exchanger consisting of a 200 m long copper tube located in a 400 l water tank at ambient temperature (20 °C). The maximum flow rate accessible with this configuration is close to 6.7 l min^{-1}. An extended discussion on the hydraulic system performances is presented below (section 3.3.1).

2.3. Instrumentation

The water temperature elevation (ΔT) is measured using two temperature probes (four wires, class A PT100) paired in a Wheatstone bridge. An additional probe is used to measure the absolute temperature of the water at the entrance of the calorimeter (T_{IN}). The flow rate measurement is made using a calibrated magnetic induction *TZN 20-05* turbine. It provides a sinusoidal electrical signal with frequency directly proportional to the flow rate (30 Hz for 1 l min^{-1}). The absolute uncertainty on the turbine measurement (including non-linearity) is better than 0.2% in the range 2 l min^{-1} to 8 l min^{-1}.

The electrical power is deduced from voltage (U_{m1}) and current measurements across the electrical heater. To perform an accurate current measurement, the voltage (U_{m2}) across a 10 mΩ (±0.01%) reference calibrated resistor (R_{sh}) is measured. The reference resistor derivative over one year is less than ±0.001% and its temperature dependence is less than 10 ppm °C^{-1}.

$$P_e = U_{m1} \cdot \frac{U_{m2}}{R_{sh}}. \tag{3}$$

Voltage measurements are accomplished using two calibrated 8808A Fluke voltmeters.

2.4. Traceability to the International System of Units

Laser power measurements are referenced to SI units by electrical calibrations. To quantify the uncertainties due to the traceability chain, the power balance is considered. During electrical calibration, a known input power (P_e, electrical primary standard) is dissipated in the electrical heater. Simultaneously, the temperature rise and the flow rate are measured. Because of electrical losses, a fraction of the whole electrical power measured is dissipated out of the calorimeter. Let L_e be the fraction of electrical power dissipated within the calorimeter. Because of the thermal losses, a fraction of this power is dissipated into the environment, and thus is not measured by the instruments. The fraction of the electrical power transmitted to the water cooling system is called D_e. Thus, the power balance during electrical calibration is written as

$$P_e \cdot L_e \cdot D_e = C_v (q \Delta T)_e, \tag{4}$$

with $(q\Delta T)_e$ the flow rate and temperature rise measured during the electrical calibration and C_v the water thermal capacity at constant volume.

During laser power measurements, the fraction of power absorbed within the optical cavity of the calorimeter is called L_o (the other part is called the optical losses). As in electrical mode, a fraction of this power is not transmitted to the water cooling system and, thus, is not measured by the instruments. The fraction of power absorbed by the calorimeter and transmitted to the water cooling system is called D_o. With these considerations, the laser power is written as

$$P_o \cdot L_o \cdot D_o = C_v (q \Delta T)_o. \tag{5}$$

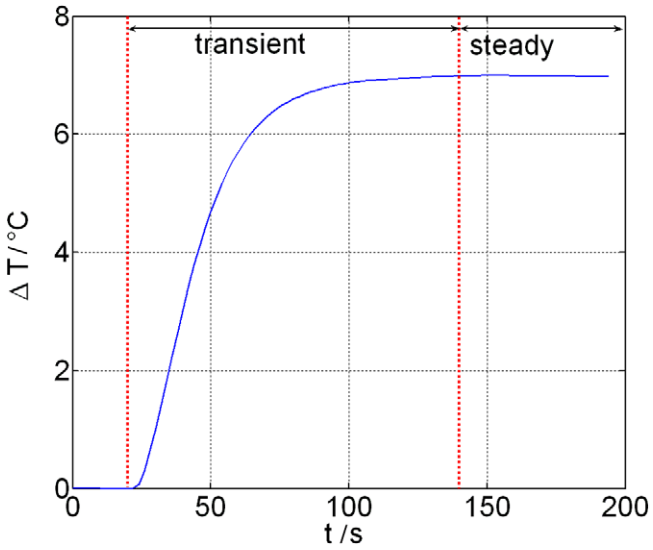

Figure 3. Example of time-dependent profile of temperature rise of water during the laser power measurement ($P = 2\,\mathrm{kW}$, $q = 4\,\mathrm{l\,min^{-1}}$).

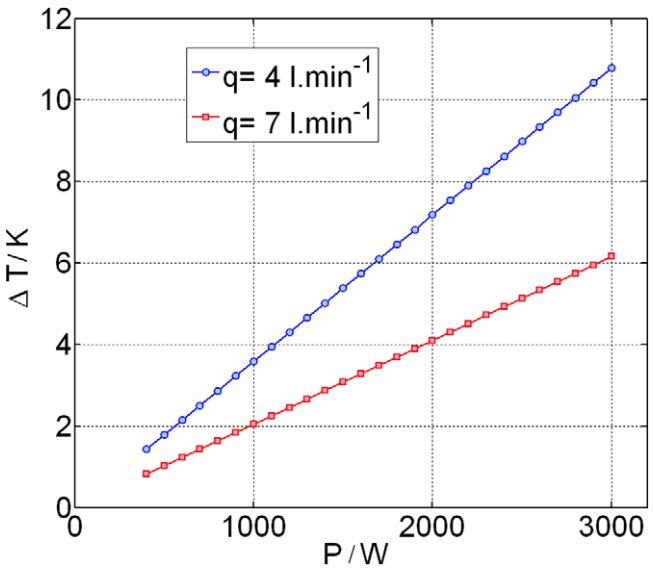

Figure 4. Temperature rise estimation for two values of flow rate.

By considering that C_v is independent of the water temperature (this assumption is discussed in section 3.2) it can be written that

$$P_o = \left[\frac{P_e}{(q\Delta T)_e}\right]\left[\frac{L_e d}{L_o}\right](q\Delta T)_o, \qquad (6)$$

with $(q\Delta T)_o$ the flow rate and temperature rise measured during the laser power measurement, and $d = D_e/D_o$ the ratio of thermal losses.

By combining equations (3) and (6) we obtain

$$P_o = \left[\frac{U_{m1}.U_{m2}}{R_{sh}(q\Delta T)_e}\right]\left[\frac{L_e d}{L_o}\right](q\Delta T)_o. \qquad (7)$$

Equation (7) is the product of three terms. The first one is composed of the measurements performed during electrical calibration. The second one is the uncertainty linked to the design of the calorimeter (it involves thermal non-equivalence, electrical and optical losses). The third one is the measurements during optical calibration. To sum up, equation (7) comes from equations (1) and (2) with a term taking the uncertainty contributors linked to the calorimeter design into account.

3. Uncertainties linked to the measurement procedure

Figure 3 shows an example of the time-dependent temperature rise profile. The temperature difference increases slowly during the settling time (transient). When ΔT remains constant over time, a steady state is reached (generally after 120 s). All the measured quantities for electrical calibrations or laser power measurements are means over 60 s in the steady state. Since the water thermal capacity is well known (see [20]), the theoretical temperature rise for different values of flow rate and power can be computed (see figure 4). Results show that the value of the flow rate strongly impacts the temperature rise. For example, when 2 kW is supplied within the calorimeter, the temperature rise is close to 7 °C for a $4\,\mathrm{l\,min^{-1}}$ flow rate, and close to 4 °C for a $7\,\mathrm{l\,min^{-1}}$ flow rate. The flow rate value has to be optimized to reduce the global uncertainty in the optical power range targeted.

3.1. Uncertainty on the primary electrical standard

The electrical primary standard requires an absolute electrical power measurement. A stable continuous voltage supply is used to dissipate a voltage within the calorimeter heater. The voltage supply is specially manufactured and designed for RLCYC 75 applications. It is a linear power supply with 2 kW serial regulation (10 A max). It allows the supply of five power levels: 320 W, 670 W, 1090 W, 1520 W and 2040 W. The electrical power is determined from the measurements of U_{m1} and U_{m2} and the standard resistor's known resistance. The expanded uncertainty on the nominal resistance of the reference resistor is 0.01%, and the power dissipated in the resistor is 0.4 W. To avoid the uncertainty linked to the increase in reference resistor temperature, air-forced convective cooling with a ventilator is implemented. The influence of current leaks on the electrical power estimation linked to the voltmeter is estimated to be less than 0.005%. The expanded uncertainty on voltmeter measurements is 76 mV for U_{m1} and 18.5 µV for U_{m2}. Since measurements used for electrical power primary standard estimation need to be absolute, the voltmeters and the standard resistor have to be calibrated in an accredited traceable laboratory.

The standard uncertainty on electrical power estimation is presented in figure 5. The relative uncertainty on electrical power measurement ranges from 0.1% to 0.04% when the electrical power ranges from 320 W to 2040 W. The main contributors are the voltage measurements (90%). In the following, it will be considered that the relative standard uncertainty on a 2 kW primary electrical standard is 0.05%.

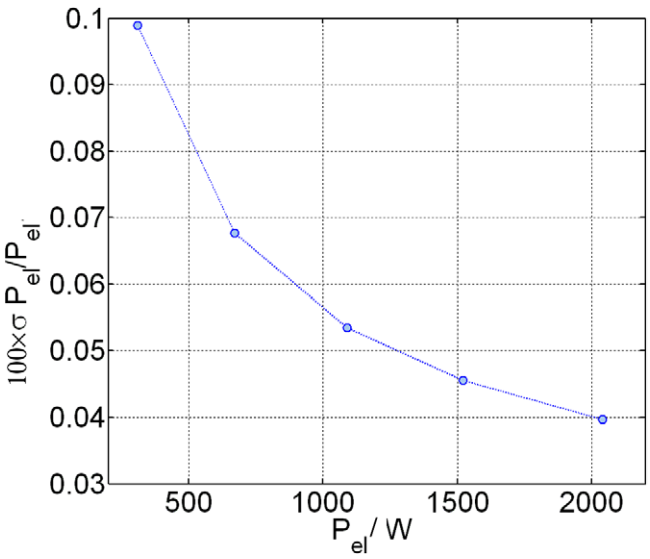

Figure 5. Relative uncertainty estimation on electrical power dissipated (primary electrical standard).

3.2. Uncertainty linked to the linear assumption

The model used for laser power estimation is based on a linear assumption (see equation (1)). This point implies that the variation of water thermal capacity at constant volume as a function of temperature is neglected. Actually, the water thermal capacity ranges from 0.069 82 kJ/(l min^{-1} K^{-1}) to 0.069 64 kJ/(l min^{-1} K^{-1}) when the water temperature ranges from 20 °C to 28 °C (relative variation of 0.3%). This is the reason why electrical power used for the calibration procedure must be of the same order of magnitude as the measured laser power. For example, with an electrical primary standard close to 2 kW, the linear assumption leads to an uncertainty of less than 0.01% in a range of laser power measured from 1900 W to 2100 W. Since our main objective is to measure 2 kW laser power, the uncertainty linked to the linear assumption is neglected in the following. This point has to be taken into account for higher power laser measurements.

3.3. Uncertainty linked to stability conditions

Since all the measurements are achieved under steady-state conditions the variation of parameters during the acquisition process leads to an uncertainty. The hydraulic system characteristics and the electrical power stability are investigated.

3.3.1. Hydraulic system stability. The uncertainty sources of the hydraulic system are the flow rate and the temperature of the water at the entrance of the calorimeter. Figure 6 shows the acquisition of T_{IN} and q for 300 s. During the 60 s acquisition process, the water temperature variation is close to 0.005 °C and the flow rate variation is close to 0.002 l min^{-1}. These performances are measurable because of the high-resolution instruments used on RLCYC 75 (0.001 °C for ΔT and 0.001 l min^{-1} for q). Since the temperature variation is higher than the flow rate variation, it is possible to increase the signal-to-noise ratio by enhancing the temperature rise measurement. Thus, it is considered that the optimum is reached by using a flow rate of 4 l min^{-1}. This configuration leads to a temperature rise close to 7 °C; the temperature variation is then close to 0.1% of the total temperature rise and the flow rate variation is close to 0.05% of the flow rate value. The variation on power measurement caused by the hydraulic system stability is estimated by the GUM technique [21], which is less than 0.12%. It can be noted that the hydraulic system stability is not a direct uncertainty contributor but it impacts the repeatability of measurements.

3.3.2. Electrical power stability. During the electrical calibration process, electrical power stability is a requirement. Figure 7 presents an example of the normalized time-dependent profiles of electrical power and temperature rise. Since the trends of both curves are very close, it can be concluded that the variation of electrical power impacts the temperature rise with a very low thermal inertia. Since the calibration procedure is much longer than the thermal inertia, the influence of electrical power variation during the calibration procedure has no influence on calibration coefficient estimation (less than 0.001%).

3.4. Uncertainty linked to temperature rise and flow rate measurements

Because of the calibration procedure, absolute measurements of the product of flow rate and temperature rise ($q \cdot \Delta T$) are not required. Nonetheless, measurement repeatability and linearity impact the global uncertainty of RLCYC 75. To study the metrological characteristics of these two measurements, repeatability campaigns with electrical and optical power are conducted.

3.4.1. Electrical campaign. To quantify the repeatability on the $q \cdot \Delta T$ product, the procedure consists in measuring the calibration coefficient ten times in the optimal configuration ($P_e = 2$ kW, $q = 4$ l min^{-1}). The standard deviation on C_e measurement is less than 0.1%.

To quantify the linearity two experimental campaigns are conducted.

- The calibration coefficient is estimated for the five values of electrical levels. The non-linearity is less than 0.25% in the range 320 W to 2040 W.
- The calibration coefficient is estimated for two flow rate regimes (4 l min^{-1} and 7 l min^{-1}). This procedure leads to a temperature rise 1.5 times lower (see figure 4); nonetheless, the calibration coefficient remains constant at 0.15%.

3.4.2. Optical campaign. To conduct optical campaigns, a divergent square-shaped laser beam from a Yb : YAG continuous laser ($\lambda = 1030$ nm) operating from 0.3 kW to 8 kW is used as the power source. In order to measure the laser power characteristics, a beam splitter is placed in the laser path to direct a small part of the laser power (8%) to

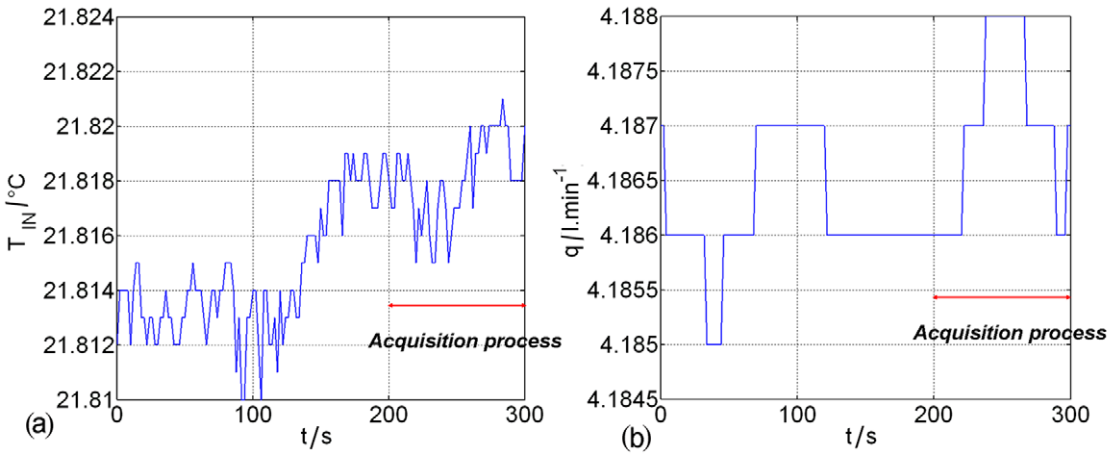

Figure 6. Visualization of the stability hydraulic system characteristics: (a) temperature at the calorimeter entrance T_{IN}, (b) flow rate at the calorimeter entrance q.

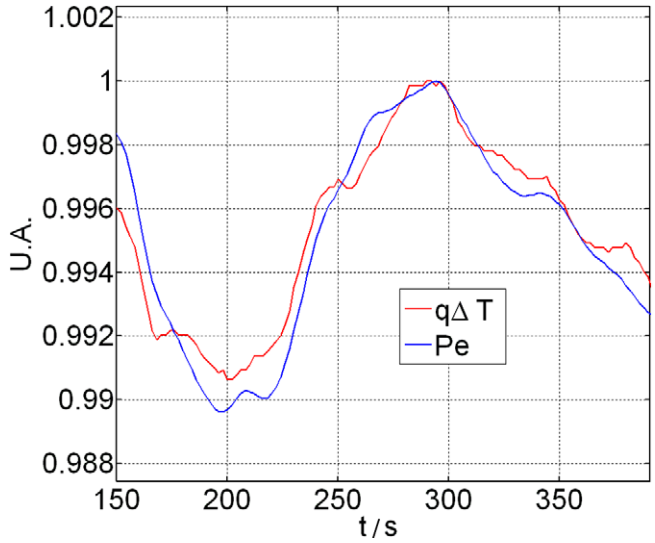

Figure 7. Non-dimensional time-dependent profiles of electrical power and temperature rise.

an InGaAs photodiode situated in an integrating sphere. To quantify instrumentation repeatability, the ratio of (calorimeter measurement) over (InGaAs measurement) is computed while a 2 kW continuous laser power is dissipated within the cavity of the calorimeter. Over ten measurements the standard deviation of this ratio is 0.15% (a part of this measurement is due to photodiode repeatability).

To study the linearity both procedures carried out in electrical modes are repeated.

- The non-linearity on measurement ratio is less than 0.25% when the laser power ranges from 500 W to 2500 W.
- The flow rate change from 4 l min^{-1} to 7 l min^{-1} leads to a change in the measurement ratio by less than 0.3%.

3.4.3. Conclusion on flow rate–temperature rise measurements. For both deposition modes, the repeatability of standard deviation is close to 0.15%. In both cases the standard deviation measured is not only due to the $q \cdot \Delta T$ product, but also due to the repeatability of power supplies. Considering that the standard deviation measured is due to the $q \cdot \Delta T$ product leads to an overestimation of the uncertainty. The standard deviation linked to the instrument repeatability is 0.15%.

The non-linearity is less than 0.25% when the power ranges from 500 W to 2000 W. Thus, in the following it is considered that the instrumentation non-linearity has no impact on the measurements in the range from 1900 W to 2100 W.

4. Estimation of electrical losses

Electrical losses (L_{e}) are defined as the fraction of electrical power measured with the electrical device (voltmeters + calibrated resistor) but dissipated outside the calorimeter (external power). In fact, the electrical junctions with voltage supply are situated outside the calorimeter. The external electrical resistance is about 0.1% of the total electrical heater resistance (40 Ω). In steady state, the power within the external part can be dissipated by natural convection of the air around the calorimeter or transmitted to the calorimeter by thermal conduction within the electrical heater. A thermal computation shows that the external power is transmitted to the calorimeter mainly by thermal conduction. Thus, during electrical calibration the fraction of electrical power dissipated in the electrical heater outside the calorimeter can be neglected (less than 0.02%). In the following, the uncertainty contribution due to electrical losses is neglected ($L_{\mathrm{e}} = 1$).

5. Estimation of optical losses

Optical losses can lead to a systematic error on RLCYC 75. To quantify this issue two methods have been implemented:

- a 3D Monte Carlo ray-tracing code (Matlab®);
- experimental procedure to perform measurements with different optical cavity apertures.

5.1. Numerical approach

5.1.1. Principle. A 3D model is developed to compute ray trajectories within the optical cavity. The ray envelope

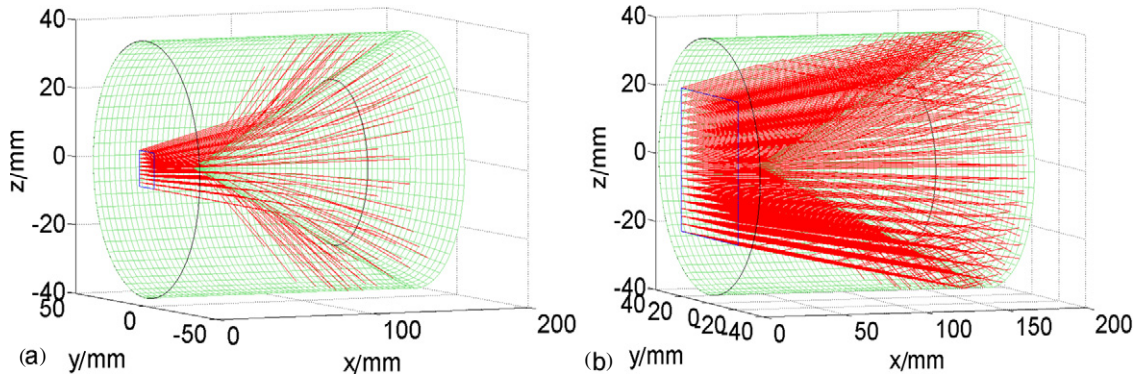

Figure 8. Visualization of ray trajectories within the calorimeter optical cavity: (*a*) side of the section beam, 10 mm; (*b*) side of the section beam, 40 mm.

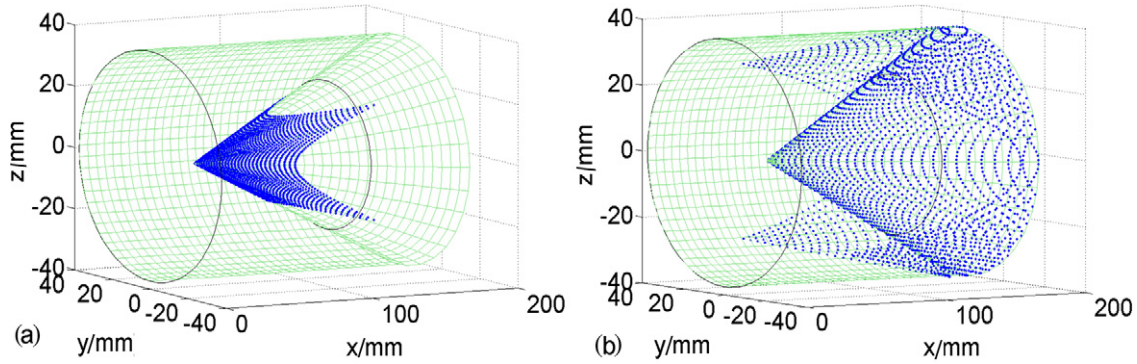

Figure 9. Ray impacts on the cavity wall: (*a*) side of the section beam, 10 mm; (*b*) side of the section beam, 40 mm.

is a divergent square-shaped laser beam. The cavity walls are meshed with a regular grid. To perform modelling of ray trajectories, the algorithm is as follows.

(1) Initial conditions: each ray is defined by a direction vector and entrance coordinates.
(2) Intersections with cavity walls are computed (if no intersection is possible, the ray is considered out of the cavity: optical losses).
(3) The direction vectors after reflection are computed.
(4) Back to step (2) until the total number of reflections is reached (seven reflections are computed).

Two assumptions are considered to compute the direction vector after reflection: specular reflections and isotropic (Lambertian) reflections. On the cavity walls, the nature of the reflection depends on the angle of incidence of the ray on the cavity wall. If it is more than 75°, specular reflections are considered. If not, isotropic reflections are considered. The decisive angle for using specular or isotropic reflections (75°) is estimated by a bidirectional reflection distribution function (BRDF) measurement on the cavity coating. In fact, BRDF results show that if the incident angle is more than 75° the main part of the power is reflected along the specular direction. In the specular reflection case, a deterministic model based on the Snell–Descartes law is used. In the isotropic reflection case, a Monte Carlo procedure is implemented: the direction vector characteristics are chosen randomly. In order to reduce the numerical uncertainty due to the numerical random process, the trajectories of 200 000 rays are computed.

5.1.2. Results. Figures 8 and 9 provide, respectively, the examples of beam splitting and ray impacts within the optical cavity for two different values of laser beam cross section. Since the model computes the ray impacts on the cavity walls, it provides an estimation of optical deposition geometry. The evolution of the numerical estimation of optical losses as a function of the laser beam size is presented in figure 10. The model predicts that the optical losses are less than 0.12% irrespective of the laser beam size. It is noteworthy that the enhancement of the laser beam size leads to a reduction in optical losses (less than 0.06% when the laser beam size is more than 30 mm). The uncertainty on the numerical estimation of optical losses is known by computing the model sensitivity to the wall absorption coefficient. It is known that the wall absorption coefficient is between 0.9 and 0.95. This value leads to an uncertainty on the model prediction close to 0.1%. That is why, in the following, the uncertainty on the estimation of optical losses is assumed to be a rectangular distribution whose length is 0.25%.

5.2. Measurement of optical losses

In order to measure the influence of optical losses, laser power measurements are carried out with different apertures of the cavity. Diaphragms are used to change the aperture side. Since the inner side of the diaphragms reflects light, the optical losses are trapped in the cavity. Thus, the use of the diaphragm leads to a laser power enhancement proportional to the optical losses. Experimental results show that the reduction of 80% in the

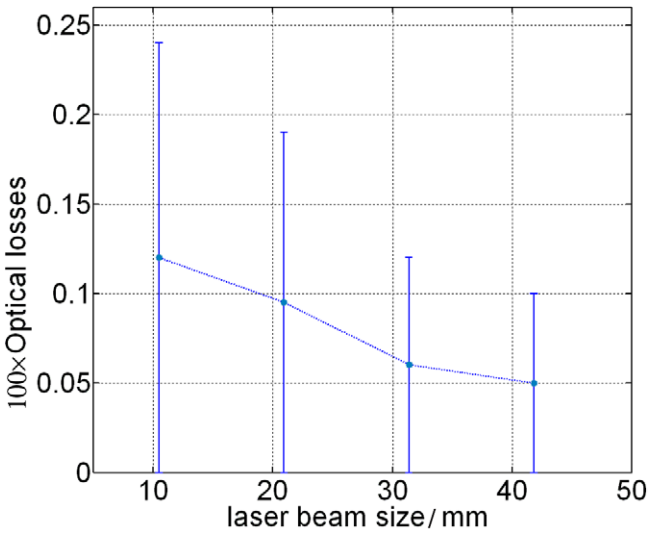

Figure 10. Optical losses as a function of the laser beam size.

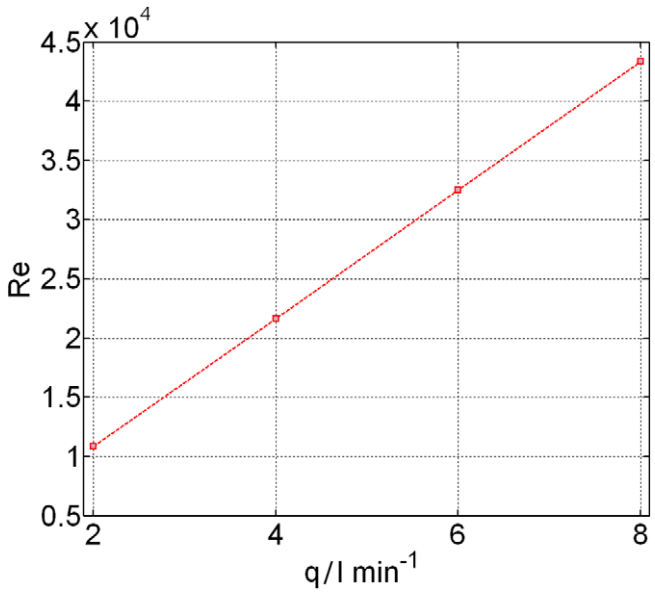

Figure 11. Evolution of the Reynolds number as a function of the flow rate.

surface aperture has an impact of less than 0.08% on laser power measurements. The uncertainty on the experimental estimation of optical losses is due to the repeatability of the $q \cdot \Delta T$ product measurement (0.15%, see section 3.3).

5.3. Conclusion on optical losses

Simulations and measurements of the optical losses lead to the same conclusion: optical losses are less than 0.25% (this result includes the uncertainty on the estimation of optical losses). This study validates the design of the optical cavity. It is possible to reduce the uncertainty on the estimation of optical losses by measuring the absorbing coating characteristics more precisely.

6. Thermal non-equivalence estimation

To study thermal equivalence, a 3D model is developed using *Comsol Multiphysics*.

6.1. Thermal model

The aim of the thermal model is to quantify thermal losses during electrical calibrations and during laser power measurements. The simulations are performed under the steady-state condition. The system discretization includes a tetrahedral mesh. A refined mesh is used on the important temperature gradient zones (cone and cylinder); a coarser mesh is used for the rest of the system.

6.1.1. Heat sources. Both electrical and optical power supplies are modelled. In electrical mode, the heat source is modelled using a surface heat source condition located on the calorimeter/electrical heater contact. Concerning optical mode, the heat source strongly depends on the impact of the laser beam within the optical cavity. In order to take into account the influence of light reflections inside the cavity the results from the ray-tracing model are used (see figure 9).

6.1.2. Modelling of convective cooling. The turbulent hydraulic cooling is modelled by estimating the convective coefficient and taking into account the temperature rise along the fluid path. Since the water cooling system consists of a square-shaped tube, the convective coefficient (h_C) value is estimated using the empirical law defined in [20]:

$$Nu = \frac{h_C \cdot D}{k} = 0.027 Re^{4/5} Pr^{1/3} \left(\frac{\mu}{\mu_s}\right)^{0.14}, \qquad (8)$$

where Nu is the Nusselt number, Re is the Reynolds number, Pr is the Prandtl number, μ is the viscosity, k is the thermal conductivity and D is the hydraulic diameter. All the quantities are estimated at water temperature except the quantity with subscript s, which is estimated at the wall temperature. The evolution of the Reynolds number and the convective coefficient as a function of the flow rate are, respectively, presented in figures 11 and 12. The flow is turbulent ($Re > 10\,000$) when the flow rate is higher than $3\,\mathrm{l\,min^{-1}}$. This point enhances the cooling convective coefficient, which ranges from $5000\,\mathrm{W\,m^{-2}\,K^{-1}}$ to $14\,000\,\mathrm{W\,m^{-2}\,K^{-1}}$ when the flow rate ranges from $2\,\mathrm{l\,min^{-1}}$ to $8\,\mathrm{l\,min^{-1}}$.

6.1.3. Modelling of thermal losses. Thermal losses due to conduction, convection and radiation are considered in the model. Thermal losses due to conduction are very low and are not described here.

Two kinds of natural convective losses must be distinguished: the convection around the outer surface of the calorimeter (external convection) and the convection within the optical cavity (internal convection). Concerning external convection a global exchange coefficient (h_{cnl}) is estimated using the classical model of natural convection around the cylinder (see [20]). It is noteworthy that the calorimeter is located in a rectangular box, which reduces the convective losses. Concerning the internal convective losses the 3D air

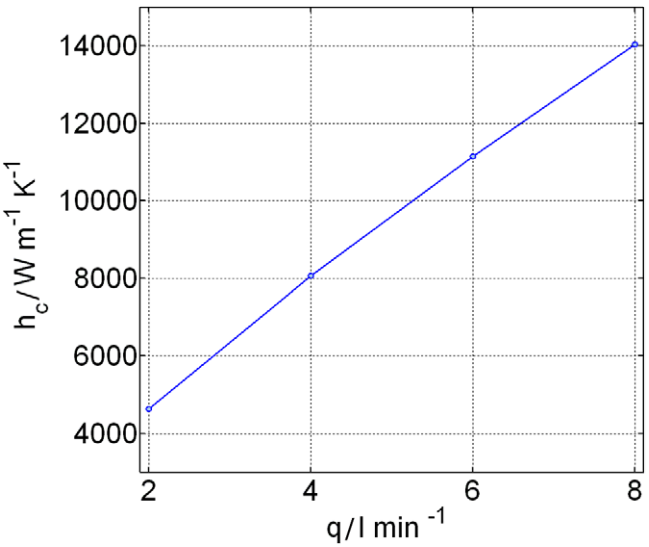

Figure 12. Evolution of the convective coefficient as a function of the flow rate.

motion is estimated in order to estimate a global convective coefficient. Results show that the effect of internal convection occurs at the cylinder entrance. Thus, internal convection does not play an important role in the whole internal surface of the cavity.

Radiation losses inside the optical cavity are modelled using a surface to surface radiation simulation while radiation losses from the outer surface are modelled using a surface to ambient radiation.

6.2. *Results and analysis*

Calorimeter temperature fields computed using the model during a 2 kW electrical calibration and during a 2 kW laser deposition are, respectively, presented in figures 13 and 14 (the flow rate is 4 l min^{-1}). The main difference between the two deposition modes is linked to the heat source location. The electrical power is supplied within the system, while optical absorption is located on the optical cavity surface. This point leads to very different thermal behaviours.

6.2.1. Comparison between numerical and experimental results. Eight temperature probes (PT 100) located at different points of the system provide measurements used to validate the thermal model. The first six probes are located along the cylinder width. The other two are located at the back of the calorimeter. The location of the probes is presented in figure 15. The measurements are acquired during a 2 kW electrical calibration and during a 2 kW optical supply. In both cases the flow rate is close to 4 l min^{-1}.

Figures 16 and 17 show that the numerical results and measurements are in good agreement since the difference between the numerical and measured results is less than 0.5 °C. This comparison validates the water cooling efficiency and the geometry of the laser deposition.

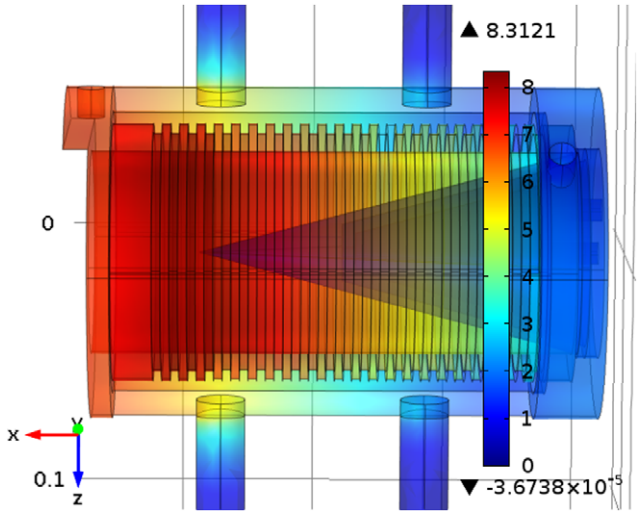

Figure 13. Visualization of the temperature field inside the calorimeter during 2 kW electrical calibration.

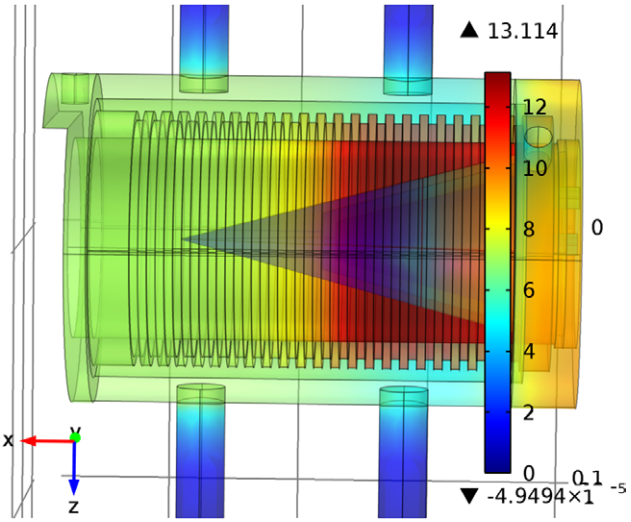

Figure 14. Visualization of the temperature field inside the calorimeter during 2 kW laser supply.

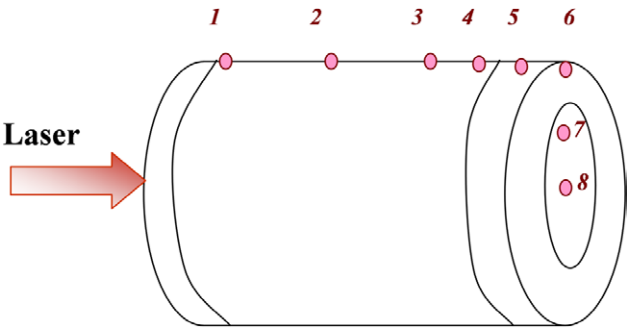

Figure 15. Location of the eight temperature probes.

6.2.2. Thermal equivalence estimation. In order to estimate the uncertainty on laser power measurements due to thermal non-equivalence the parameter ε is defined:

$$d = 1 + \varepsilon \tag{9}$$

with d the term defined in equation (7).

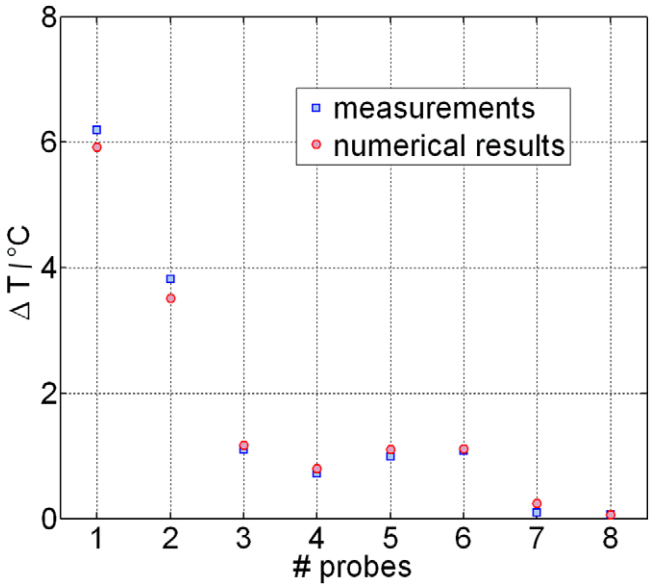

Figure 16. Comparison between PT 100 measurement and numerical results in electrical mode.

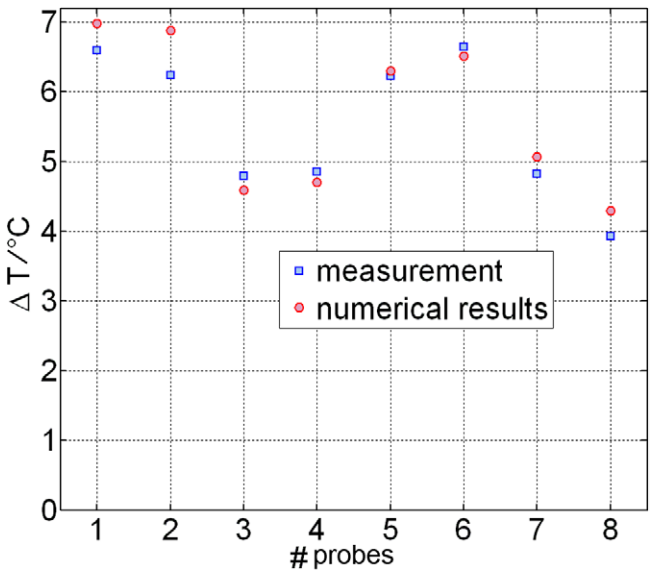

Figure 17. Comparison between PT 100 measurement and numerical results in optical mode.

Figures 18 and 19 show the evolution of the parameter ε as a function of the power and flow rate. The ε value is less than 0.08% in the range of power from 500 W to 2000 W. The model shows that the fraction of thermal losses is very close in the two deposition modes. The main part of thermal loss is due to convection (70%). To sum up, the hydraulic system is sufficiently well designed to perform an efficient cooling whatever the heat source location. The ε value ranges from 0.15% to 0.05% when the flow rate ranges from $2\,\mathrm{l\,min^{-1}}$ to $6\,\mathrm{l\,min^{-1}}$. The difference in terms of thermal non-equivalence when the flow rate ranges from $4\,\mathrm{l\,min^{-1}}$ to $6\,\mathrm{l\,min^{-1}}$ is less than 0.02%. This point justifies the use of a $4\,\mathrm{l\,min^{-1}}$ flow rate for accurate measurements.

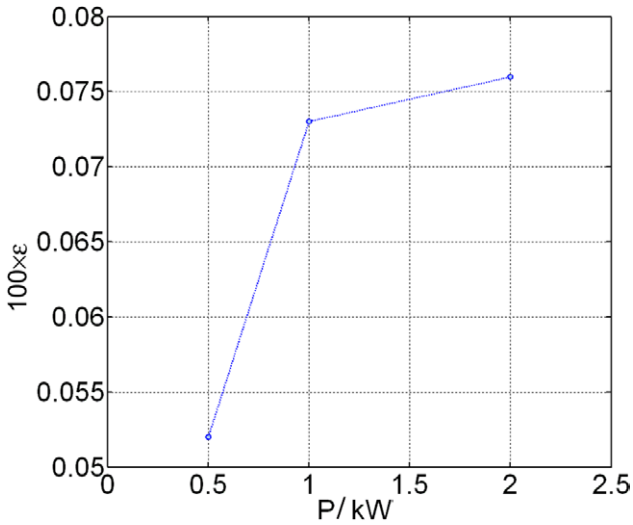

Figure 18. Evolution of parameter ε as a function of the power ($q = 4\,\mathrm{l\,min^{-1}}$).

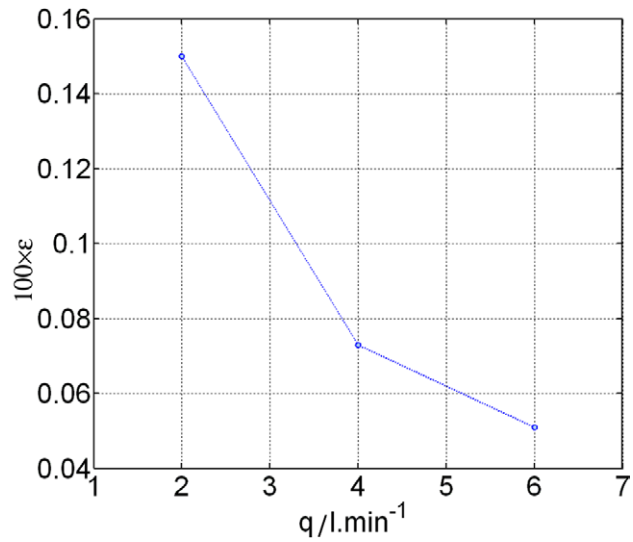

Figure 19. Evolution of parameter ε as a function of the flow rate ($P = 2\,\mathrm{kW}$).

6.2.3. Uncertainty associated with thermal equivalence estimation. To quantify the uncertainty on ε estimation, the sensitivity of the model parameters is investigated. Some parameters used in the model are not perfectly known: the fraction of power deposited on the cylinder in optical mode (R_S), the convective coefficient value for water cooling (h_C) and the convective coefficients for natural convection cooling (h_{cn1} for external convection, h_{cn2} for internal convection). The influence of these parameters is presented in table 1.

With these values the uncertainty on the numerical estimation of ε is estimated to be less than 0.1%. Thus, in the following, the uncertainty due to thermal non-equivalence is assumed to be a rectangular distribution whose length is 0.2%.

7. Uncertainty associated with laser power measurement

To determine the uncertainty on laser power measurement the error sources are separated into type A and type B

Table 1. Range and influence of parameters on numerical estimation of ε.

Parameters	Value range	Influence on ε estimation
R_S	10%–20%	0.03%
h_C	6000 W m^{-2} K^{-1} to 10 000 W m^{-2} K^{-1}	0.02%
h_{cn1}	2 W m^{-2} K^{-1} to 5 W m^{-2} K^{-1}	0.05%
h_{cn2}	0 W m^{-2} K^{-1} to 3 W m^{-2} K^{-1}	0.02%

Table 2. Uncertainty contributors.

Uncertainty contributors	Typical value in nominal conditions	Standard deviation (σ)	Type	Section in this paper
P_e	2000 W	0.05%	Type B	3.1
U_{m1}	288 V	0.026%	Type B	3.1
U_{m2}	70 mV	0.026%	Type B	3.1
R_{sh}	0.01 Ω	0.01%	Type B	3.1
Linear model assumption	0	0.01% (neglected)	X	3.2
$(q\Delta T)_o$	28 K l min^{-1}	0.15%	Type A	3.4
$(q\Delta T)_e$	28 K l min^{-1}	0.15%	Type A	3.4
L_e	1	0.02% (neglected)	Type B	4
L_o	0.9988	0.072%	Type B	5
d	1.001	0.058%	Type B	6

errors. Type A uncertainties are the ones whose magnitude is estimated by computing the standard deviation (σ_A) over a series of measurements. Type B uncertainties are estimated using a non-statistical method (modelling or theoretical). Concerning type B, a rectangular uncertainty distribution is assumed. Let a be the length of the rectangular distribution, the standard deviation (σ_B) is then estimated by the equation

$$\sigma_B = \frac{a}{2\sqrt{3}}. \tag{10}$$

The results are given in table 2.

The expanded ($k = 2$) uncertainty on laser power measurement, called $U(P)$, is then the quadratic sum of the standard deviation of each contributor multiplied by 2:

$$U(P) = 2\sqrt{\sum \sigma_A^2 + \sum \sigma_B^2}. \tag{11}$$

The expanded uncertainty ($k = 2$) on absolute laser power measurement is then 0.5%. The weight of the contributors is presented in figure 20. In total, 65% of the global uncertainty is statistical uncertainty due to the instrumentation. This value includes the contribution of the hydraulic system stability. The uncertainty estimation procedure is accomplished for 5 kW laser power measurement. The uncertainty is then close to 0.9% (the enhancement is mainly due to the error linked to the linear assumption).

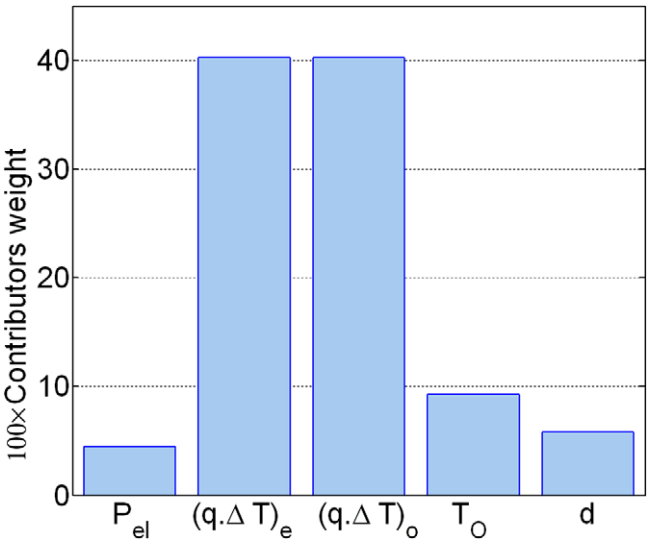

Figure 20. Weight of relative contributors.

8. Conclusion

The RLCYC 75 is a new electrically calibrated laser power calorimeter especially manufactured for LMJ optical diagnostic calibration at 2 kW, 1 µm. In this study, all the uncertainty sources on laser power measurements traceable to the International System of Units are investigated numerically or experimentally. To this end, two numerical models are developed and experimental campaigns are conducted. The uncertainties on model results are taken into account. The expanded uncertainty ($k = 2$) on absolute power measurement is found to be 0.5% at 2 kW.

The error sources are separated into instrumentation uncertainties and uncertainties due to calorimeter design. It appears that 80% of the global uncertainty is due to the instrumentation repeatability, which includes the stability of our hydraulic system. Thus, to reduce the uncertainty of our traceability chain, the measurement campaign procedure has to be improved.

Concerning uncertainty due to the calorimeter design (thermal non-equivalence and optical losses), results can be compared with cryogenic calorimeter performances presented in [15, 19]: the thermal non-equivalence is found to be less than 0.0004% and optical losses are close to 0.002%. Nonetheless,

by calibrating RLCYC 75 at 2 kW, the improvement in our approach consists in considering that the magnitude enhancement of these contributors is compensated by a reduction in the traceability chain. To the best of our knowledge, no other institute has performed electrical calibration of a 1 µm standard laser calorimeter in this range of power.

Concerning calorimeter design optimization, two main improvements are planned. To enhance thermal equivalence, an insulated enclosure has been designed to reduce thermal losses. To reduce the uncertainty on optical loss estimation, the absorbing coating characteristics will be measured with a higher accuracy. Moreover, a reduction in optical aperture using a diaphragm can be implemented.

To validate our primary standard accuracy, international comparisons of high laser power measurements have to be achieved with standards of metrology institutes.

References

[1] Néauport J, Journot E, Gaborit G and Bouchut P 2005 Design, optical characterization, and operation of large transmission gratings for the laser integration line and laser mega joule facilities *Appl. Opt.* **44** 3143–52

[2] Hocquet S, Penninckx D, Bordenave E, Goudéard C and Jaouën Y 2008 FM to AM conversion in high power lasers *Appl. Opt.* **47** 3338–49

[3] www.lmj.cea.fr

[4] Brandt F, Kück S and Grütz A 2010 Traceable laser power measurements of diode laser radiation in the near infrared *MAPAN—J. Metrol. Soc. India* **25** 29–35

[5] Li X, Scott T R, Cromer C L, Brandt F and Möstl K 2000 Power measurement standards for high-power lasers: comparison between the NIST and the PTB *Metrologia* **37** 445–7

[6] Li X, Scott T, Yang S, Cromer C and Dowell M 2004 Nonlinearity measurement of high power laser detectors at NIST *J. Res. Natl Inst. Stand. Technol.* **109** 429–34

[7] Lehman J, Cromer C, Yang S and Dowell M 2006 Review of ultraviolet and high power laser measurement standards at NIST *Simposio de Metrologia (25–27 October 2006, Santiago de Queretaro, Mexico)*

[8] Soscia M 1990 Calorimétrie laser: mesure de fortes puissances laser *LNE, Bulletin du BNM* no 82

[9] Hadler J, Cromer C L and Lehman J H 2007 NIST measurement services: cw laser power and energy calibrations at NIST *NIST Special Publication* 250-75

[10] Li X, Hadler J, Cromer C L, Lehman J H and Dowell M 2008 NIST measurement services: high power laser calibrations at NIST *NIST Special Publication* 250-77

[11] Möstl K 1989 Laser power and energy radiometry, new developments and applications in optical radiometry *Inst. Phys. Conf. Ser.* **92** 1–18

[12] West E D and Schmidt L B 1977 System for calibrating laser power meters for the range 5–1000 W *National Bureau of Standards Technical Note* p 685

[13] Franzen D L and Schmidt L B 1976 Absolute reference calorimeter for measuring high power laser pulses *Appl. Opt.* **15** 3115–22

[14] Thacher P D 1976 Calorimeters for pulsed lasers: calibration *Appl. Opt.* **15** 1815–22

[15] Gentille T R, Houston J M, Hardis J E, Cromer C L and Parr A C 1996 National Institute of Standards and Technology high accuracy cryogenic radiometer *Appl. Opt.* **35** 1056–68

[16] Martin J E, Fox N P and Key P J 1985 A cryogenic radiometer for absolute radiometric measurements *Metrologia* **21** 147–55

[17] Jauniskis L, Foukal P and Kochling H 1992 Absolute calibration of an ultraviolet spectrometer using a stabilized laser and a cryogenic cavity radiometer *Appl. Opt.* **31** 5838–43

[18] Chen D H and Zhang Z M 2000 Thermal analysis of the volume absorber in pulsed excimer laser calorimeters *Int. J. Heat Mass Transfer* **43** 3061–72

[19] Livigni D J, Cromer C L, Scott T R, Johnson B C and Zhang Z M 1998 Thermal characterization of a cryogenic radiometer and comparison with a laser calorimeter *Metrologia* **35** 819–27

[20] Incorpera F and DeWitt D 1990 *Fundamentals of Heat and Mass Transfer* 3rd edn (New York: Wiley)

[21] BIPM 2008 *Evaluation of Measurement Data—Guide to the Expression of Uncertainty in Measurement (GUM)* JCGM 100:2008; downloadable on www.bipm.org or *ISO/IEC Guide* 98-3